

Spatial and temporal resolution of metabolic dysregulation in the Sugen hypoxia model of pulmonary hypertension

Catherine E. Simpson¹  | Anjira S. Ambade¹ | Robert Harlan² | Aurelie Roux² | David Graham² | Neal Klauer¹ | Tijana Tuhy¹  | Todd M. Kolb¹ | Karthik Suresh¹  | Paul M. Hassoun¹ | Rachel L. Damico¹

¹Johns Hopkins University Division of Pulmonary and Critical Care Medicine, Baltimore, Maryland, USA

²Johns Hopkins All Children's Hospital Molecular Determinants Core, St. Petersburg, Florida, USA

Correspondence

Catherine E. Simpson, Johns Hopkins University Division of Pulmonary and Critical Care Medicine, 1830 E. Monument St., Fifth Floor, Baltimore, MD 21205, USA.
 Email: catherine.simpson@jhmi.edu

Funding information

Pulmonary Hypertension Association, Grant/Award Number: Aldrighetti Young Investigator Award; National Scleroderma Foundation, Grant/Award Number: New Investigator Award; National Heart, Lung, and Blood Institute, Grant/Award Numbers: K08HL132055, K23HL153781, R01HL132153

Abstract

Although PAH is partially attributed to disordered metabolism, previous human studies have mostly examined circulating metabolites at a single time point, potentially overlooking crucial disease biology. Current knowledge gaps include an understanding of temporal changes that occur within and across relevant tissues, and whether observed metabolic changes might contribute to disease pathobiology. We utilized targeted tissue metabolomics in the Sugen hypoxia (SuHx) rodent model to investigate tissue-specific metabolic relationships with pulmonary hypertensive features over time using regression modeling and time-series analysis. Our hypotheses were that some metabolic changes would precede phenotypic changes, and that examining metabolic interactions across heart, lung, and liver tissues would yield insight into interconnected metabolic mechanisms. To support the relevance of our findings, we sought to establish links between SuHx tissue metabolomics and human PAH -omics data using bioinformatic predictions. Metabolic differences between and within tissue types were evident by Day 7 postinduction, demonstrating distinct tissue-specific metabolism in experimental pulmonary hypertension. Various metabolites demonstrated significant tissue-specific associations with hemodynamics and RV remodeling. Individual metabolite profiles were dynamic, and some metabolic shifts temporally preceded the emergence of overt pulmonary hypertension and RV remodeling. Metabolic interactions were observed such that abundance of several liver metabolites modulated lung and RV metabolite-phenotype relationships. Taken all together, regression analyses, pathway analyses and time-series analyses implicated aspartate and glutamate signaling and transport, glycine homeostasis, lung nucleotide abundance, and oxidative stress as relevant to early PAH pathobiology. These findings offer valuable insights into potential targets for early intervention in PAH.

This is an open access article under the terms of the Creative Commons Attribution-NonCommercial License, which permits use, distribution and reproduction in any medium, provided the original work is properly cited and is not used for commercial purposes.

© 2023 The Authors. *Pulmonary Circulation* published by John Wiley & Sons Ltd on behalf of Pulmonary Vascular Research Institute.

KEYWORDS

metabolism, -omics, pulmonary arterial hypertension

INTRODUCTION

Pulmonary arterial hypertension (PAH) is a progressive disease characterized by elevated pulmonary vascular resistance leading to right ventricular (RV) remodeling and culminating in right heart failure.^{1–3} PAH is, in part, a disease of disordered metabolism, and high-throughput metabolomics has emerged as a powerful tool for comprehensively investigating metabolic perturbations associated with disease.^{4–7} Metabolomics studies in clinical PAH have revealed abnormalities in lipid metabolism, energy metabolism, and amino acid metabolism, however, most prior human studies have examined metabolites in serum or plasma at a single point in time, which may not sufficiently reflect fundamental disease biology.^{8–11} Circulating metabolites likely underrepresent the dynamic metabolic changes that occur within and across relevant tissue beds, and cross-sectional studies cannot address causal associations. At present, it is not clear which metabolic derangements in human PAH are cause versus consequence of disease.

The Sugen hypoxia (SuHx) rodent model of PAH closely mimics human disease, and is therefore frequently used to study PAH pathobiology.^{12–15} In contrast to human studies, studies utilizing experimental PH models enable access to the heart and lung tissues that primarily manifest disease. Furthermore, animal models can be studied longitudinally over compressed time courses, in contrast to long follow-up periods required to capture meaningful endpoints in clinical cohorts. Importantly, prior studies indicate shared metabolic dysregulation between experimental PH in rodents and human PAH.^{12,16–18} However, no previous studies have comprehensively examined metabolic evolution over time as PH develops in the SuHx model, and only one prior study, performed in a murine PH model, assessed tissue metabolism in bulk heart and lung tissues.¹⁹

In the current study, we leverage targeted tissue metabolomics to examine tissue-specific relationships between evolving metabolism and pulmonary hypertensive features over time in the SuHx model. We hypothesized that for some metabolic perturbations, metabolic change would precede pulmonary pressure elevation and RV remodeling, from which we might begin to infer which elements of metabolic reprogramming are positioned upstream of pathobiologic

effects. We further hypothesized that metabolic activity in a given tissue type might potentiate metabolism in other tissue types, and therefore, by examining metabolic interactions across heart, lung, and liver tissues, we might gain more comprehensive insight into interconnected metabolic mechanisms regulating disease.

METHODS

Complete methods are available in the Online Supplement.

Hemodynamic assessment and tissue acquisition

All animal experiments were performed in accordance with the National Institutes of Health Guide for the Care and Use of Laboratory Animals and were approved by the Animal Care and Use Committee of The Johns Hopkins University School of Medicine. Male Wistar rats (250–275 g) were injected subcutaneously with the VEGFR2 inhibitor SU5416 (20 mg/kg) (TOCRIS, 3037; Tocris Bioscience) on Day 1. Rats were then placed in a hypoxia chamber for predefined time periods before sacrifice (7, 14, and 21 days). Normoxic control rats were injected with SU5416 vehicle on Day 1 and kept in room air next to the hypoxic chamber. On Days 7, 14, and 21, six experimental and six control rats were anesthetized with intraperitoneal injection of ketamine (50 mg/mL/kg) and xylazine (Rompun) (5 mg/mL/kg). An open-chest approach was used to measure right ventricular systolic pressure (RVSP) in anesthetized rats as previously described.^{20,21} After hemodynamic measurements were completed, the chest cavity was opened immediately and the heart was excised rapidly and placed in ice-cold 0.9% normal saline to remove any blood. Under a dissecting microscope, the atria and extraneous vascular material were removed from the heart. The RV wall was carefully separated from the left ventricle and the septum, and both portions were blotted dry and weighed. Fulton index was calculated as the ratio of the weight of the RV to left ventricle plus septum (RV/LV + S); the RV mass index (RVMI) was calculated as the ratio of RV weight to body weight. Lung and liver were similarly excised and blotted dry.

Tissue preparation and liquid chromatography-mass spectrometry

Sample preparation was performed by pulverizing tissue samples using a Precellys Evolution Homogenizer & Cryolys Evolution Cooling Unit (Bertin Corp). Sample filtration was accomplished using a Versa 1100 Liquid Handling System (Aurora Biomed). Ten microliters of each filtered sample was pooled together into a Quality Control (QC) POOL to be run alongside the samples at regular intervals. Twenty-five microliters of filtrate were further diluted with 75 μ L of water (Fisher Chemical Optima™ LC/MS, W6) with heavy internal standards before analysis by LC-MS/MS. Liquid chromatography-mass spectrometry (LC-MS) was performed by injecting samples, blanks, and QC Pools at varying injection volumes based on the signal strength of each sample type on the LC-MS system. The high-pressure liquid chromatography (HPLC) procedure employed a Shimadzu HPLC system, which included a SIL-30ACMP 6-MTP Autosampler and Nexera LC-30AD HPLC Pumps (Shimadzu). Chromatographic separation was achieved using a pentafluorophenyl-propyl (PFPP) column, measuring 150 \times 2.1 mm ID with a 3 μ m particle size (567503-U; Sigma). A triple quadrupole (QQQ) mass spectrometer (LCMS-8060; Shimadzu) with an electrospray ionization source was used for mass spectrometry in both positive and negative modes. A System Suitability QC, created from commercially available plasma and extracted using the laboratory's sample preparation method, was run with each batch of samples. Batches that passed QC analysis were subsequently used for metabolite analyses.

Statistical analysis

For all tissues, metabolites with >50% missingness were filtered out. Metabolite abundances between groups (e.g., control vs. SuHx) and across tissue types were compared using fold-change analyses, unpaired *t* tests of differences, and one-way analysis of variance, as appropriate. No data transformation or scaling methods were applied before univariate analyses. Before multivariate analyses, missing metabolite values were replaced using one-fifth of the minimum positive value for a given metabolite.^{22,23} Metabolite data were rescaled such that the mean abundance was set to 0 and the standard deviation set to 1 to generate *z*-scores. Principal component analyses (PCA) and partial least squares discriminant analyses (PLS-DA) were performed for dimensionality reduction.^{24,25} For PLS-DA models, the Q2 statistic was calculated to validate

predictive performance, and a *p* value for permutation tests was calculated for class prediction accuracy.²⁶ Variable importance in projection (VIP) coefficients were generated for metabolite features driving model component projections. Multivariate empirical Bayes time-series analysis (MEBA) was performed to examine metabolic time-course differences between groups. Hotelling T² statistics were calculated for each metabolite time-course, with a high Hotelling T² score indicating a significant difference in mean metabolite slope between SuHx and control. Simple linear regressions were used to examine associations between metabolites and animal hemodynamics and RV measurements. Interaction terms were added for analysis of metabolite-by-metabolite interactions across tissue types. Elastic net regression, a form of lasso regression suited to best subset variable selection among correlated variables, was used to identify parsimonious models predictive of phenotypic features (RVSP, RV weight, etc).^{27,28} Pathway analysis was performed to contextualize metabolite results, with the KEGG library used as a back-end reference. Metabolite set enrichment analysis (MSEA) was performed using lung tissue data to predict dysfunctional enzymatic pathways.²⁹ To explore potential links to human disease, the Gene Expression Omnibus (GEO) site was searched for metabolomic and transcriptomic datasets derived from human PAH lung studies, and molecules implicated by MSEA results were queried.³⁰ All analyses were performed using Stata version 17 and the *MetaboAnalystR* package for R, version 5.0.^{31,32}

RESULTS

Disease development in the animal model

Pulmonary hypertensive changes developed in SuHx animals in a step-wise fashion, with significant differences in SuHx compared with control animals noted by Day 7 (Figure 1 and Supporting Information: Table 1). By Day 21, RVSP had risen to an average of 61 mmHg (\pm 12 mmHg) in the SuHx group, consistent with established PH. RV remodeling in the SuHx model lagged RVSP rise, with an increase in RV weight that was numerically but not significantly higher in SuHx at Day 7. By Day 21, Fulton index was 0.60 in SuHx animals, consistent with substantial RV remodeling, compared with 0.26 in control animals. With disease established, SuHx animals had significantly higher average hematocrit and significantly lower average liver weight compared with control animals (Supporting Information: Table 1).

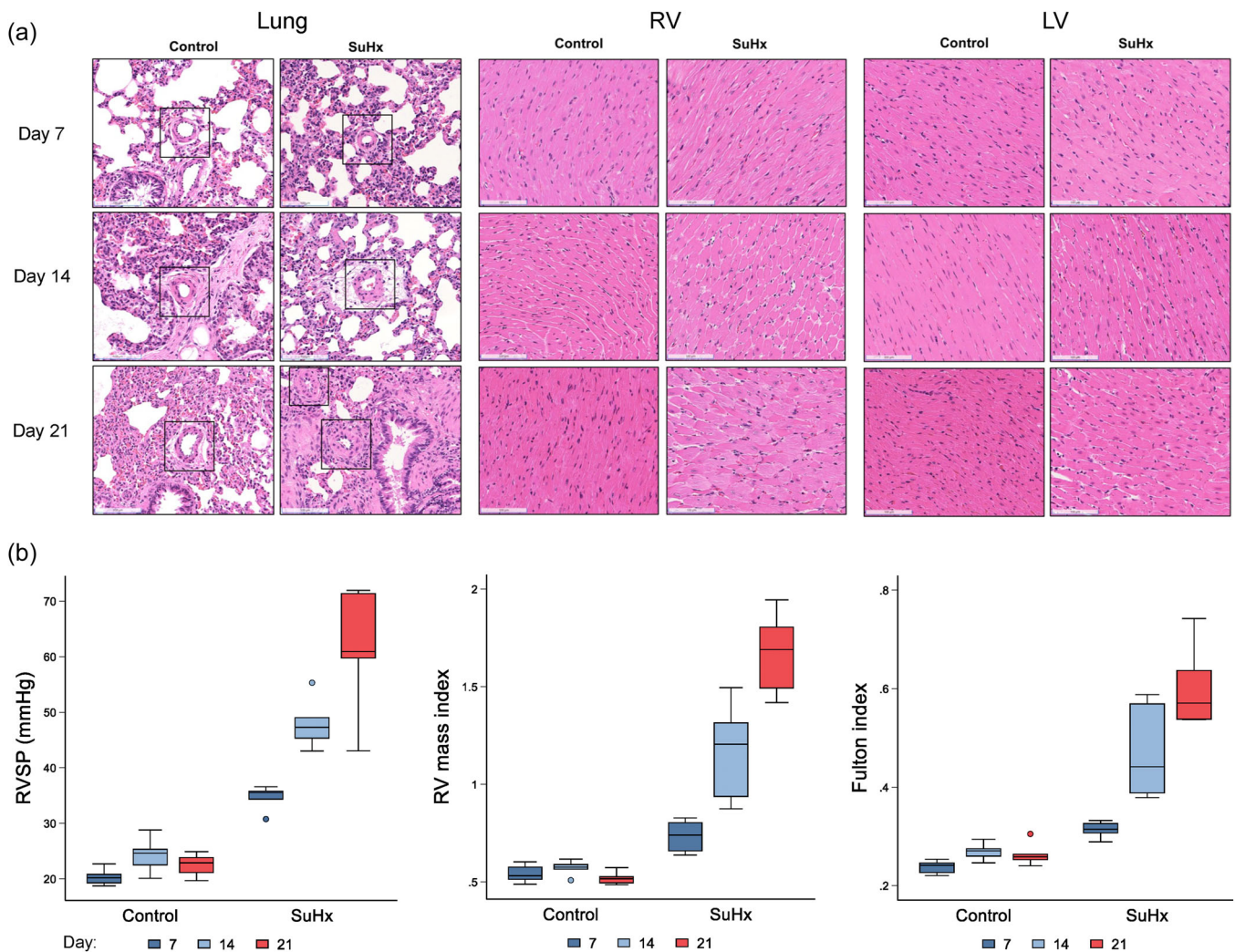


FIGURE 1 (a) Representative hematoxylin and eosin (H&E) stained images of lungs, right ventricle (RV) and left ventricle (LV) from control and SuHx rats at Days 7, 14, and 21 showing remodeling of pulmonary vasculature (lungs) and hypertrophied cardiomyocytes (RV and LV). (Magnification: $\times 20$, Scale bar = $100 \mu\text{m}$). (b) Box and whisker plots demonstrating changes in RVSP, RV mass index (RV mass adjusted for body weight), and Fulton index for SuHx versus control animals at Weeks 1, 2, and 3 postinduction with Sugen. Horizontal lines within the box represent the median, upper and lower bounds of the box represent 75th and 25th percentiles, respectively, and whiskers represent upper and lower fences. Data points beyond upper and lower fences are plotted individually as dots. RVSP, right ventricular systolic pressure.

Metabolic differences between and within tissue types

PCA of 330 metabolite features detected across tissues demonstrated substantial separation in scores space according to tissue type (Supporting Information: Figure 1). For each of the four tissue types examined (lung, RV, LV, liver), PLS-DA produced clear separation between SuHx and control animals in scores space, implying distinct tissue-specific metabolism in experimental PH (Figure 2). Individual metabolites driving component projection within each tissue type are shown in VIP plots in Figure 3. For each tissue type, metabolism had evolved significantly in SuHx compared with control

animals by Day 7, and the two conditions remained distinctly metabolically different over the time course studied (Supporting Information: Figures 2 and 3).

FC differences for individual metabolites varied substantially by tissue type and over time (Supporting Information: Figure 4). FC patterns for some tissue metabolites aligned with metabolic patterns known to exist in the circulation, while for other metabolites, FC directionality in the tissue was opposite the circulation. For example, in the PAH lung, a brisk rise in nucleotides was observed, which is similar to metabolic dysregulation captured in the circulation.⁸ This increase was evident by Day 7 and persisted through Day 21. A similar pattern of persistent elevation in the

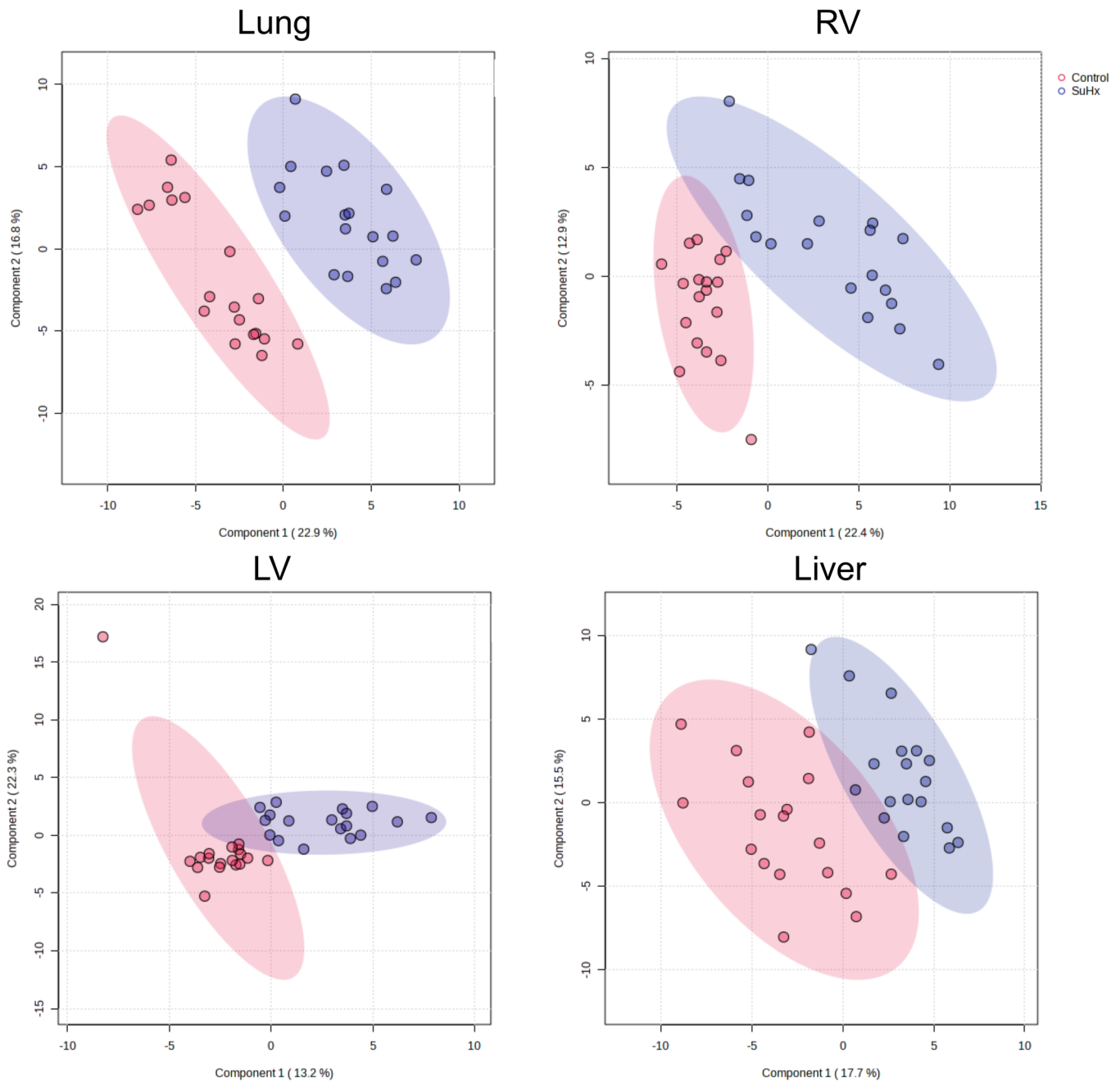


FIGURE 2 Scores plots depicting results of partial least squares discriminant analysis of lung, RV, LV, and liver metabolites in SuHx versus control animals. For each model, components 1 and 2 are projected, and percent variance explained by each component is listed in parentheses. Red dots represent control animals; blue dots represent SuHx animals. LV, left ventricle; RV, right ventricle.

animal model was seen for lung acetylcarnitine, which is also observed in human circulation.⁹ By contrast, many purines (xanthine, hypoxanthine, and uric acid), lactic acid, and branched chain amino acids (valine, leucine, isoleucine), which are elevated in the PH circulation, were decreased in the PAH lung (Supporting Information: Figure 4).

Results of pathway analysis for lung and RV tissue metabolomics are shown in Figure 4a. Upregulated beta-alanine metabolism, alanine, aspartate and

glutamate metabolism, and nicotinamide metabolism were seen in the PAH lung. Arginine biosynthesis, arginine metabolism, glutamine and glutamate metabolism, and glutathione metabolism were among the overrepresented pathways in both tissue types. Pathway analysis results for LV and liver tissue metabolomics are shown in Figure 4b. Histidine metabolism was highly significantly upregulated in the LV. In the liver, arginine biosynthesis and metabolism were significantly upregulated.

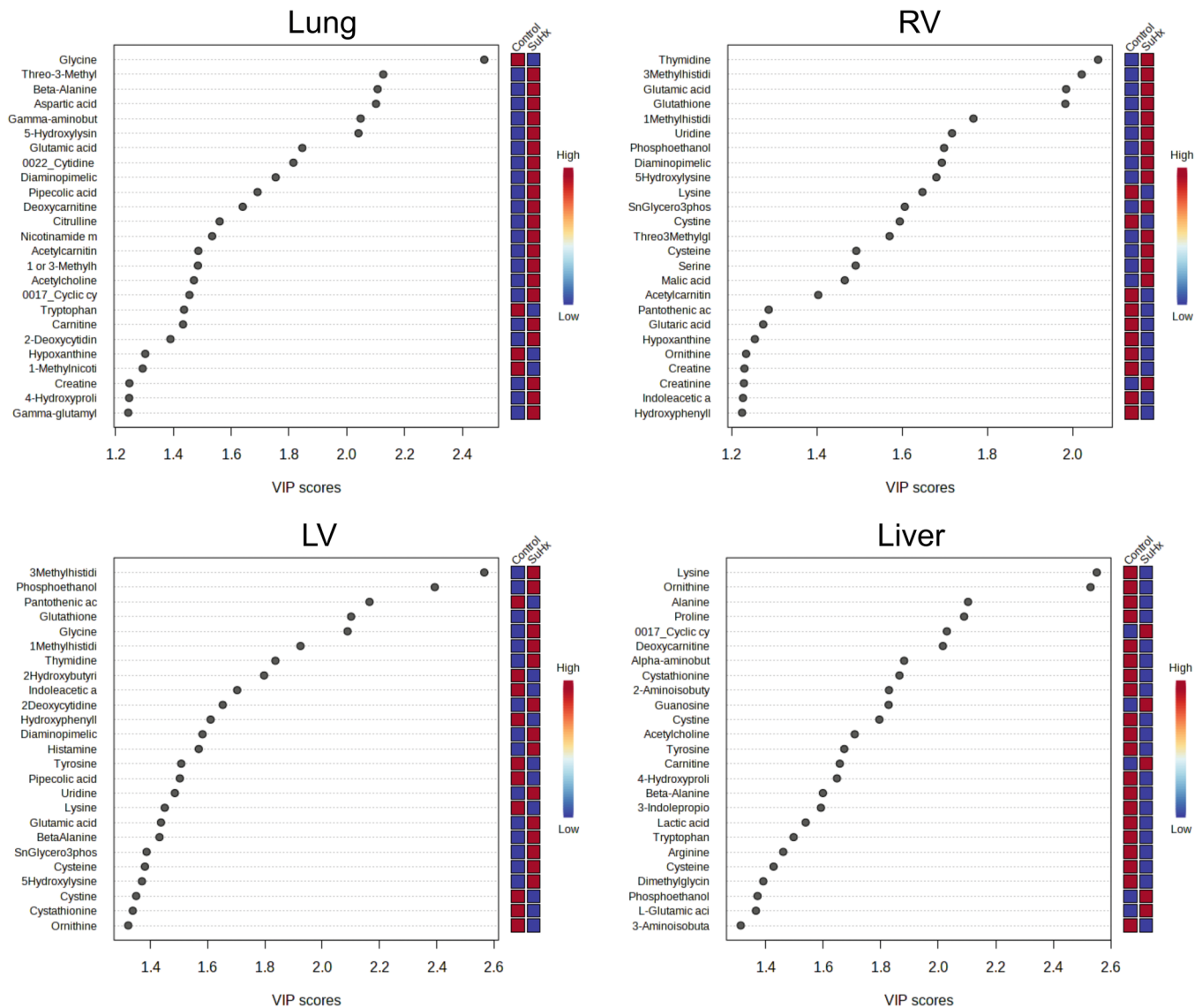


FIGURE 3 Variable importance in projection plots showing VIP scores for individual metabolites resulting from the PLS-DA models depicted in Figure 2. VIP scores convey the relative importance of a particular metabolite in discriminating between conditions (e.g., SuHx vs. control). The bars to the right of the dot plots convey relative metabolite abundance in SuHx versus control. PLS-DA, partial least squares discriminant analyses; VIP, variable importance in projection.

Tissue-specific associations with hemodynamics and RV remodeling

We focused our analyses of metabolite-phenotype associations on the lung and RV tissues in SuHx, as these are the organs that primarily manifest disease in PAH. Lung metabolite features that were significantly associated with RVSP, RV weight indexed to body weight, and Fulton index are shown in the dot plots in Figure 5a, sorted by strength of association with RVSP. Lung metabolite-phenotype associations were notable for a high frequency of purine and pyrimidine nucleotides, proteinogenic amino acids, and branched chain amino acids (leucine, isoleucine, valine) significantly

associated with RVSP. RV metabolite-phenotype associations, shown in Figure 5b, were notable for associations with phospholipid intermediates (Sn-glycero-3-phosphocholine, phosphoethanolamine), and markers of oxidative stress (glutathione, cysteine).

Elastic net regression was performed to define parsimonious models, consisting of linear combinations of metabolite features, accounting for a high proportion of variability in hemodynamic and RV measurements. In the lung, a combination of glycine, nicotinamide mononucleotide (an NAD⁺ precursor), gamma-aminobutyric acid (GABA), beta-alanine (a GABA agonist), and guanidoacetic acid (a precursor of creatine) explained 76% of RVSP variance

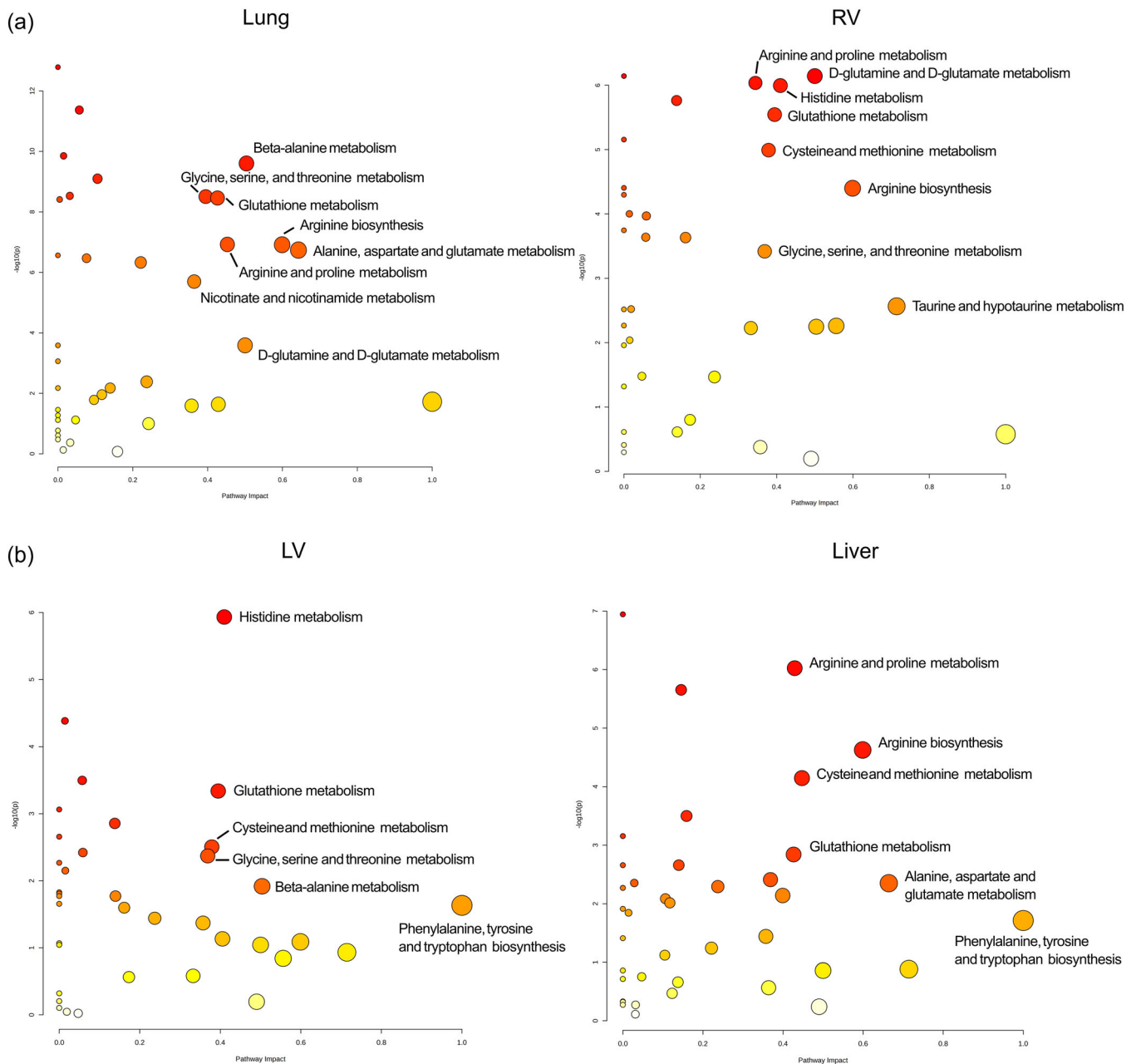


FIGURE 4 Pathway analysis for lung and RV tissue metabolomics (a) and LV and liver tissue metabolomics (b). Pathway impact is plotted on the x-axis, and significance is plotted on the y-axis. Point sizes are proportionate to pathway impact. Point colors reflect p values from largest (light yellow) to smallest (red). The KEGG pathway database was used as a reference metabolome. LV, left ventricle; RV, right ventricle.

(Supporting Information: Table 2). Among these, glycine and nicotinamide mononucleotide had the largest individual effect sizes, and these two features were independently associated with RVSP after adjustment for other explanatory metabolite variables.

In the RV, a combination of 11 metabolites was the most parsimonious subset of features for describing RVSP variability, together explaining 62% of RVSP variance (Supporting Information: Table 3). Selected

metabolites included the phospholipid intermediate Sn-glycerophosphocholine; pantothenic acid, a precursor of coenzyme A, a compound critical for fatty acid oxidation; and hydroxybutyric acid, a product of fatty acid oxidation. Glutathione and cysteine, markers of oxidative stress, were also included in the model. Interestingly, a different combination of 13 metabolite features was selected to account for variability in the Fulton index (out-of-sample $R^2 = 0.79$), a measure of RV remodeling (Supporting Information: Table 4). While

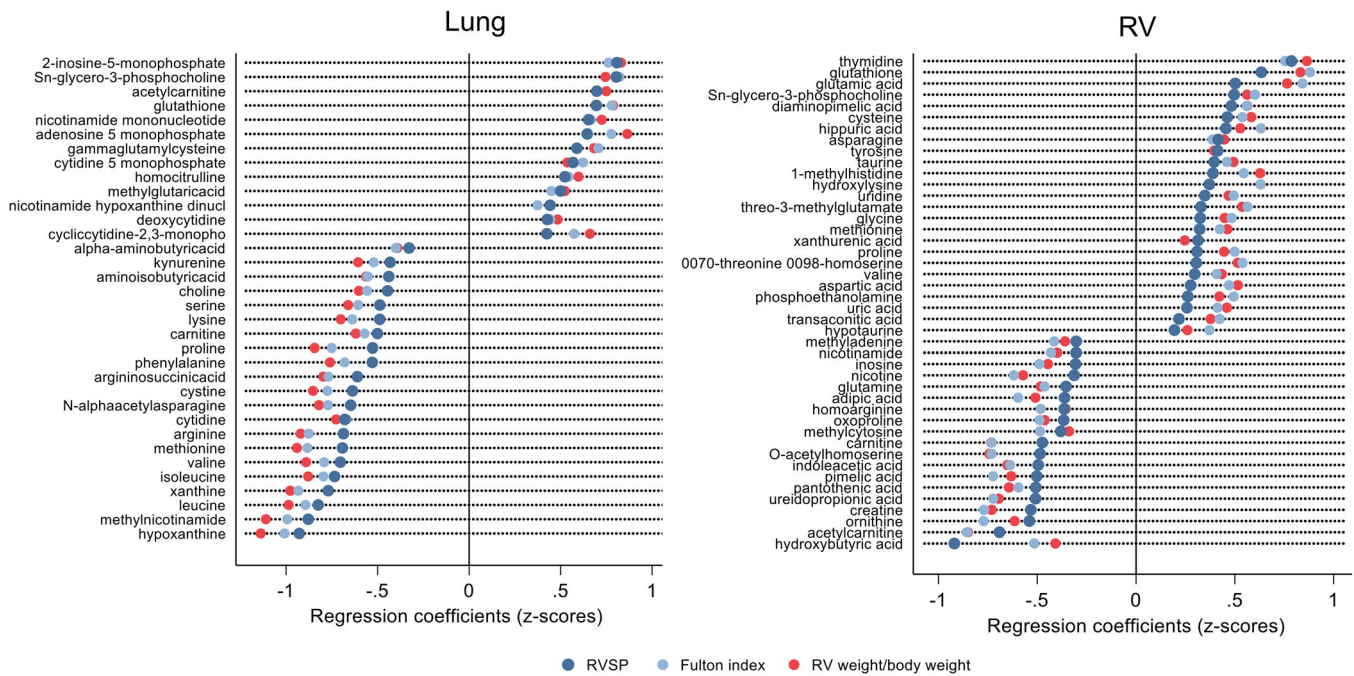


FIGURE 5 Dot plots showing regression coefficients for simple linear regression models in which individual metabolites are entered as explanatory/independent variables, and RVSP (dark blue), Fulton index (light blue), and RV mass index (red) are dependent variables. Dots represent point estimates, and the null (0) is marked by a vertical reference line. Lung models are depicted at left, and RV models are depicted at right. Metabolite abundances were entered into models as z-scores, such that 0 represents the mean abundance, +1 represents one standard deviation above the mean, and -1 represents one standard deviation below the mean. RV, right ventricle; RVSP, right ventricular systolic pressure.

some metabolites in this subset, such as glutathione and pantothenic acid, overlapped the model describing RVSP, some metabolites, including pyrimidine nucleotides, taurine, valine, and three-3-methylglutamate, were unique to the Fulton index model. Metabolites with the largest individual effect sizes for Fulton index included lysine, a proteinogenic amino acid utilized for crosslinking of collagen polypeptides and in the production of carnitine; creatine, the precursor of phosphocreatine, which is used to regenerate ATP; and glutathione.

Time-series differences and temporal comparisons with hemodynamics and RV remodeling

To focus our list of individual metabolites for temporal comparisons with pulmonary hypertensive changes, we prioritized lung and RV metabolites with time courses that significantly differed in SuHx compared with control (Supporting Information: Tables 5 and 6 and Supporting Information: Figures 5 and 6). We then leveraged volcano plots to visually identify which of the prioritized metabolites exhibited metabolic change that outpaced

phenotypic change (in RVSP, RV weight, Fulton index) by Day 7.

In the lung, four metabolites met both of the conditions we stipulated. Each rose over time in SuHx (whereas they remained flat in control animals), and the magnitude of Day 7 metabolic FC exceeded that of RVSP FC: aspartic acid, a nonessential amino acid with multiple roles in metabolism (protein synthesis, urea cycle, TCA cycle, gluconeogenesis); GABA, an inhibitory neurotransmitter synthesized from glutamate; beta-alanine, a GABA receptor agonist; and three-3-methylglutamate, which blocks glutamate transport channels in multiple tissue types. Additionally, the FC decrease in glycine exceeded the magnitude of early FC rise in RVSP (Supporting Information: Figure 7). Of these lung metabolites with significant and early FC dynamics, all were associated with RVSP in regression analysis, except for three-3-methylglutamate. Correlations between these select lung metabolites and phenotypic parameters are presented in Supporting Information: Table 7.

In the RV, metabolites with early metabolic FC were not among the metabolites with time course profiles that differed most markedly in SuHx versus control. Notable among RV metabolic Day 7 FC differences were

acetylcarnitine, which facilitates fatty acid oxidation, and markers of oxidative stress (Supporting Information: Figure 8). Many of these metabolites were significantly associated with RV weight and Fulton index in regression analysis, however, in contrast to the lung, no RV metabolic change outpaced RVSP rise or RV remodeling.

Metabolic interactions across tissues

We performed interaction analyses to understand whether relationships between metabolites in a given tissue bed (e.g., lung or heart) and associated phenotypes (e.g., RVSP or RV mass) differed with varying abundances of metabolites from other tissue beds. Our interaction analyses uncovered multiple instances in which liver metabolite abundance interacted with lung or RV metabolite-phenotype relationships. Lung glycine, which demonstrated a steep, early decline in SuHx that outpaced pulmonary hypertensive change, demonstrated statistically significant interactions with multiple liver metabolites in predicting RVSP, including NAD precursors and the proteinogenic amino acids asparagine and tyrosine. As shown in the plots in Supporting Information: Figure 9, the relationship between lung glycine and RVSP varied significantly according to abundance of these liver metabolites. Liver adenosine had a large effect on the relationship between lung glycine and RVSP, with higher levels of adenosine associated with a steeper relationship between depressed glycine and high RVSP (Supporting Information: Figure 9).

Liver cystine, a marker of oxidative stress, demonstrated interactions with several RV metabolites, including thymidine, pantothenic acid, and creatine, which were among the top RV metabolites predictive of RV remodeling in elastic net regression (Supporting Information: Figure 10). Liver acetylcarnitine also demonstrated interactions with several RV metabolites, including kynurenine; transaconitic acid; lactic acid; betaine; and glutamic acid (Supporting Information: Figure 10). The abundance of lactic acid in the liver significantly interacted with relationships between lung nucleotides and RVSP (Supporting Information: Figure 11).

Metabolites in the circulation

To investigate whether metabolic perturbations observed in the tissues might be captured in the circulation, as a posthoc analysis, we analyzed

metabolites in the plasma at the time of established disease (21 days) in SuHx animals versus controls. Plasma metabolomics facilitated discrimination of SuHx versus controls with PLS-DA, however, only four metabolites differed significantly between the two groups (Supporting Information: Figure 12). The circulating metabolites that differed significantly in SuHx reflected disease profiles of both the RV (glutathione, serine, 1-methylhistidine) and the lung (citrulline, 2-deoxycytidine).

Bioinformatic predictions and connections to human PAH

To contextualize our tissue metabolomics results and examine potential connections to human disease, we performed MSEA, leveraging lung tissue metabolites to predict dysfunctional enzymatic pathways in the PAH lung. MSEA results are shown in Figure 6, with the top-most predictions involving pathways regulating fatty acid metabolism (peroxisomal FAD transport, methenyltetrahydrofolate carboxylase, acetyl-CoA carboxylase); central carbon metabolism, including glycolysis, gluconeogenesis, pentose phosphate pathway, TCA cycle (carboxylic acid dissociation, pyruvate carboxylase, glyceraldehyde-3-phosphate dehydrogenase, etc); and altered tryptophan metabolism down the kynurenine pathway (3-hydroxy-L-kynurenine hydrolase, 3-hydroxyanthranilate-3,4-dioxygenase, kynurenine 3-monooxygenase, etc.), all metabolic pathways with observed aberrancy in human PAH. In addition, one top prediction involved glutamate transport via sodium and potassium-coupled glutamate transporters, which are not presently known to impact upon PAH pathobiology.

We cross-referenced these bioinformatic predictions with publicly available gene expression data from human PAH bulk lung tissue, focusing on genes known to regulate the metabolic pathways implicated by our analyses. *SLC1A3*, a protein-coding gene encoding the glutamate transporter EAAT1 (excitatory amino acid transporter 1, also called the glutamate-aspartate transporter 1) was significantly upregulated in PAH compared with control lungs in GEO data sets GSE53408³³ and in GSE113439³⁴ (Figure 6). *MTHFD2* and *ACACA*, which encode methenyltetrahydrofolate cyclohydrolase and acetyl-CoA carboxylase, respectively, were also significantly upregulated in the PAH lung in both data sets (Figure 6). In GSE113439, *GABRA* and *GRIN* genes encoding various GABA and NMDA receptor subunits, which are acted upon by glutamate, aspartate, and glycine, were significantly downregulated in the PAH lung (Figure 6).

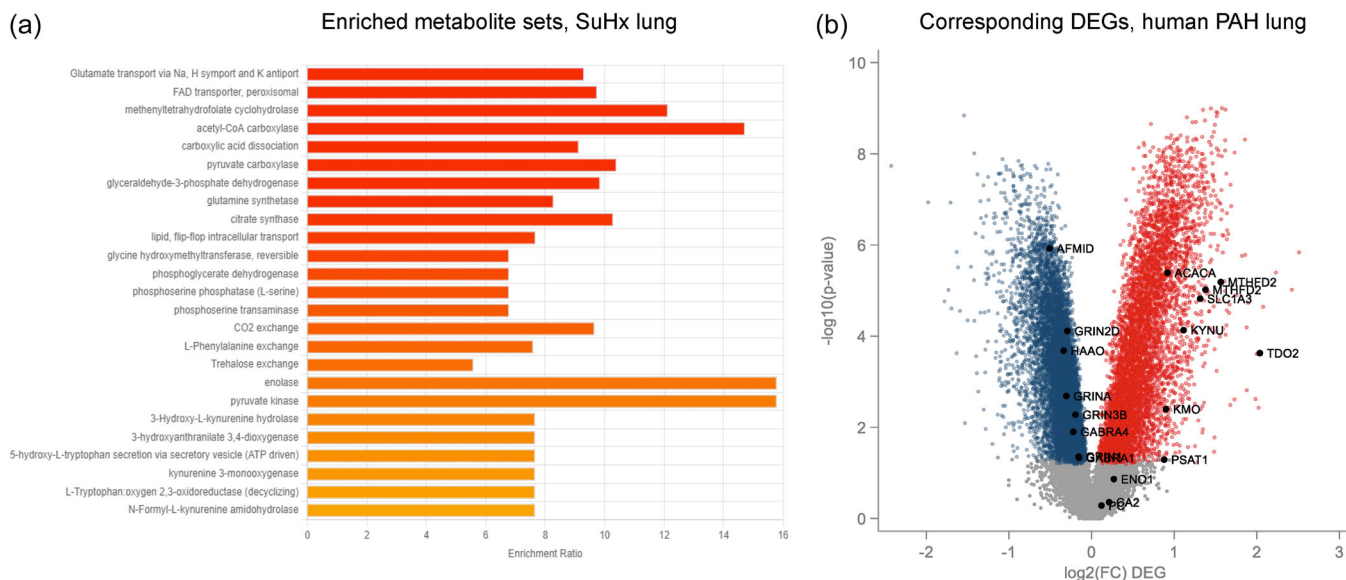


FIGURE 6 Bar plots depicting significant results from metabolite set enrichment analysis (MSEA) for rat lung tissue metabolomics (a). Enriched metabolite sets implicate dysfunctional enzymatic pathways. Enrichment ratio is calculated as observed hits/expected hits,²⁹ and red-orange spectrum of color represents the significance of the association, with redder circles showing more highly significant associations. Volcano plot depicting differentially expressed genes in human PAH lungs (compared with non-PAH controls) for pathways implicated by MSEA (b). The x-axis represents the magnitude of $\log_2(\text{fold-change})$ difference between PAH and control lungs. The y-axis represents the significance of fold-change differences as expressed by the $-\log_{10}(p\text{-value})$. Red dots represent DEGs higher in PAH, and blue dots represent DEGs lower in PAH. Gray dots represent genes with fold-change differences that do not surpass a Bonferroni-corrected threshold for statistical significance.

DISCUSSION

To our knowledge, this is the first study to examine metabolic evolution across space and time as disease develops in an experimental model that closely recapitulates human PAH. Our results show that metabolic disturbances develop as early as 1 week after PAH induction, well before pulmonary hypertensive changes are fully manifest, and that SuHx animals are metabolically distinct from control animals throughout disease development. Furthermore, we show that time course profiles are dynamic and unique for individual metabolites. Specific metabolic perturbations distinguishing SuHx from control animals vary by time point, such that individual metabolites most predictive of early disease are not necessarily the same metabolites predictive of manifest disease, an observation with important implications for clinical biomarker development.

Our use of a time course also allows examination of the temporal relationships between metabolic changes and pulmonary hypertensive changes. It is reasonable to speculate that early metabolic changes are more likely representative of pathogenic processes upstream of pulmonary vascular and/or RV remodeling, and therefore, time-course results can provide a framework for prioritizing specific metabolic pathways for additional

mechanistic investigation. What follows is a discussion of several particular metabolic processes implicated by our findings.

Glutamate transport and signaling

One of the top-most predictions resulting from MSEA analysis was dysfunctional glutamate transport, and indeed, our analysis of human bulk lung transcriptomics reveals significant upregulation of the protein-coding gene for EAAT1, the glutamate-aspartate transporter, in the human PAH lung. EAAT1 is present in human heart and lung tissues. In rat cardiomyocytes, EAAT1 overexpression increases malate/aspartate shuttle activity, and the transporter has been localized to the inner mitochondrial membrane.³⁵ Glutamate is an amino acid with a central role in energy metabolism, and glutamatergic signaling has previously been studied in PAH lungs.^{36,37} Glutamate accumulates in the pulmonary artery in human PAH, and glutamate signaling through the NMDA receptor promotes PASM proliferation.³⁶ Experiments in MCT rats have shown that NMDA receptor blockade attenuates pathologic pulmonary vascular remodeling and disrupts glutamate-NMDA receptor axis signaling.³⁶ In human precision-cut lung

slices, NMDA receptor blockade attenuates pulmonary artery contractility.³⁷

In our study, glutamate rose briskly, with a large FC increase compared with control by Day 7, then it fell in abundance by Day 14 and through Day 21. Threo-3-methylglutamate, which blocks glutamate transport via EAAT channels, was among the four metabolites that demonstrated greater metabolic FC increase than RVSP FC increase, and threo-3-methylglutamate remained significantly higher compared with control throughout the time course. Glutamate also serves as the precursor to GABA, a neurotransmitter with inhibitory effects in the central nervous system. In our lung tissue metabolomics, upregulation of GABA and beta-alanine, both GABA receptor agonists, were among the earliest metabolic changes that developed in the PAH lung, before development of pulmonary hypertension. These metabolites were also among the subset of lung metabolites most predictive of RVSP. Though GABA receptors are present in the human lung, evidence for a role for GABA signaling in PAH is scant and conflicting.^{38,39}

Glycine homeostasis

Glycine was the lung metabolite most profoundly reduced in SuHx relative to control, demonstrating a significant reduction by Day 7. Glycine remained low in SuHx compared with control over the time course, however, gradually increased in abundance in SuHx as PH progressed. Glycine was also independently and robustly predictive of RVSP, even after adjustment for other lung metabolites in the best subset of variables selected by elastic net regression. Elegant studies have established the importance of glycine homeostasis to endothelial cell biology in PAH.⁴⁰ In vitro, PAEC intracellular glycine accumulation results from deficiency of BOLA3 (Bola family member 3), which is essential to the function of the glycine cleavage system, and is associated with endothelial proliferation and vasoconstriction. Forced overexpression of BOLA3 in vivo protects against PH, however, this effect is abolished when animals are fed a diet supplemented in glycine.⁴⁰ These experiments suggest glycine homeostasis is critical to the development of PH, however specific underlying mechanisms remain unknown. Notably, previous work by our group has shown that an oxidized glutathione transpulmonary shunt exists in the SuHx animal.¹⁷ Because glycine contributes to glutathione synthesis (via glutamine), this observation raises the possibility that lung glycine depletion may occur, at least in part, in the course of glutathione synthesis and transpulmonary glutathione release.

Glycolytic shift and oxidative stress at the whole-body level

Metabolism is a complex and integrated process that involves multiple tissues and organs. The liver is the primary organ responsible for the metabolism of carbohydrates, lipids, and proteins and is a major source of reactive oxygen species (ROS) due to its high metabolic rate and involvement in detoxification processes. Our analyses suggest metabolic interactions occurring at the whole-body level may modulate elements of heart and lung metabolic reprogramming that are associated with PH development. For example, the relationship between lung glycine and RVSP varies with upregulation or downregulation of several liver metabolites, including NAD precursors and proteinogenic amino acids. These findings suggest an interplay between lung glycine metabolism and various aspects of liver metabolism, including altered bioenergetics and fluctuation of the degree to which proteinogenic amino acids are provisioned to the circulation.

Liver abundance of lactic acid, a byproduct of Warburg physiology (the shift from oxidative phosphorylation to glycolysis, known to occur in PAH), significantly interacted with a number of lung nucleotides, which may indicate that nucleotide turnover in the lung is impacted by glycolytic shift in the liver. There is evidence that lactate-derived carbons can be reintroduced, via lactate dehydrogenase A, back to acetyl-CoA.⁴¹ This mechanism is well-described in T-cells.⁴² One interpretation of our data is that liver-derived lactate may be altering the anaplerosis landscape of the lung by reshaping which fuels are supplying carbons to the TCA cycle in the context of glycolytic shift.

Cystine is the oxidized product of cysteine, and as such, is considered a surrogate for oxidative stress. Liver cystine levels demonstrated interactions with several RV metabolites that reveal significant relationships with RV hypertrophy. One interpretation of this finding is to hypothesize that the degree of whole-body oxidative stress may impact upon metabolic processes in the RV that contribute to the molecular basis of RV remodeling. Aspects of metabolism such as this are likely missed when mechanistic studies are designed in vitro.

Limitations

There are several limitations to this study that must be considered when evaluating its results. While rodents and humans share many metabolic similarities, there are interspecies differences. Some biologic pathways in animals have different regulatory mechanisms compared

with humans, and findings from experimental PH models often fail to translate to human disease. Though our study is enhanced by longitudinal metabolic time courses available for experimental and control animals, we cannot conclude causality from the temporality we demonstrate. Statistical interactions can tell us that the relationship between a particular metabolite and a particular phenotypic feature changes with varying abundance of another metabolite, but we cannot conclude effect modification, nor can we infer causality or directionality, from these interactions alone. While we can compare metabolites in the circulation to the metabolite profiles of diseased tissue beds, other organ systems and processes are also reflected by the circulation, and we must interpret findings in that context. Finally, PAH is a complex and multifactorial condition involving numerous molecular pathways and cellular processes. Therefore, the impact of manipulating one signaling pathway at a time may be subtle in human disease, and mechanistic studies *in vitro*, *in vivo*, and *in silico* that are designed to unravel complex and coordinated biologic networks are needed.

Conclusions

The tissue metabolome is altered in a time-dependent manner during disease development in the SuHx model of PAH. Metabolic reprogramming exists on a tissue-specific and whole-body level, and metabolic interactions exist across tissue types that may alter PAH pathobiology. Results from our study, taken together with observations from prior literature, show that several targetable biological processes occur very early in PAH development. Strategies for metabolic manipulation of such pathways could inform design of future clinical trials and drug development efforts.

AUTHOR CONTRIBUTIONS

Catherine E. Simpson and Rachel L. Damico designed the study. Anjira S. Ambade performed animal experiments and prepared tissue samples for metabolomics. Robert Harlan, Aurelie Roux, and David Graham performed metabolomics experiments and interpreted data. Catherine E. Simpson, Robert Harlan, Tijana Tuhy, and Neal Klauer performed statistical analysis and interpreted results. Todd M. Kolb, Karthik Suresh, and Paul M. Hassoun interpreted results and contributed important contextualizing intellectual content. Catherine E. Simpson drafted the manuscript, and all authors contributed revisions. All authors approved the final, submitted draft of the manuscript.

ACKNOWLEDGMENTS

The authors wish to acknowledge Susan Aja, PhD, for assistance with sample organization and tracking. This study was supported by the NIH/NHLBI K23HL153781 (Catherine E. Simpson), R01HL114910 (Paul M. Hassoun), U01HL125175-03S1 (Paul M. Hassoun), R01HL132153 (Rachel L. Damico, Paul M. Hassoun), K08HL132055 (Karthik Suresh), New Investigator Award from the Scleroderma Foundation (Catherine E. Simpson).

CONFLICT OF INTEREST STATEMENT

Dr. Paul M. Hassoun serves on a scientific steering board for MSD, an activity unrelated to the current work. Dr. Rachel L. Damico has received payments for expert witness testimony regarding unrelated matters. The remaining authors declare no conflict of interest.

DATA AVAILABILITY STATEMENT

Data will be made available upon reasonable request to the corresponding author.

ETHICS STATEMENT

All animal experiments were performed in accordance with the National Institutes of Health Guide for the Care and Use of Laboratory Animals and were approved by the Animal Care and Use Committee of The Johns Hopkins University School of Medicine.

ORCID

Catherine E. Simpson  <http://orcid.org/0000-0002-2388-5660>

Tijana Tuhy  <http://orcid.org/0000-0002-8922-9471>

Karthik Suresh  <http://orcid.org/0000-0003-2920-0949>

REFERENCES

- Hassoun PM. Pulmonary arterial hypertension. *N Engl J Med*. 2021;385:2361–76. <https://doi.org/10.1056/NEJMr2000348>
- Humbert M, Kovacs G, Hoepfer MM, Badagliacca R, Berger RMF, Brida M, Carlsen J, Coats AJS, Escribano-Subias P, Ferrari P, Ferreira DS, Ghofrani HA, Giannakoulas G, Kiely DG, Mayer E, Meszaros G, Nagavci B, Olsson KM, Pepke-Zaba J, Quint JK, Rådegran G, Simonneau G, Sitbon O, Tonia T, Toshner M, Vachery JL, Vonk Noordegraaf A, Delcroix M, Rosenkranz S. 2022 ESC/ERS Guidelines for the diagnosis and treatment of pulmonary hypertension. *Eur Respir J*. 2022;61:2200879. <https://doi.org/10.1183/13993003.00879-2022>
- Simonneau G, Montani D, Celermajer DS, Denton CP, Gatzoulis MA, Krowka M, Williams PG, Souza R. Haemodynamic definitions and updated clinical classification of pulmonary hypertension. *Eur Respir J*. 2019;53:1801913. <https://doi.org/10.1183/13993003.01913-2018>
- Fessel JP, Hamid R, Wittmann BM, Robinson LJ, Blackwell T, Tada Y, Tanabe N, Tatsumi K, Hemnes AR, West JD.

- Metabolomic analysis of bone morphogenetic protein receptor type 2 mutations in human pulmonary endothelium reveals widespread metabolic reprogramming. *Pulm Circ.* 2012;2:201–13. <https://doi.org/10.4103/2045-8932.97606>
5. Assad TR, Hemnes AR. Metabolic dysfunction in pulmonary arterial hypertension. *Curr Hypertens Rep.* 2015;17:20. <https://doi.org/10.1007/s11906-014-0524-y>
 6. Paulin R, Michelakis ED. The metabolic theory of pulmonary arterial hypertension. *Circ Res.* 2014;115:148–64. <https://doi.org/10.1161/CIRCRESAHA.115.301130>
 7. Lewis GD. The emerging role of metabolomics in the development of biomarkers for pulmonary hypertension and other cardiovascular diseases (2013 Grover Conference series). *Pulm Circ.* 2014;4:417–23. <https://doi.org/10.1086/677369>
 8. Rhodes CJ, Ghataorhe P, Wharton J, Rue-Albrecht KC, Hadinnapola C, Watson G, Bleda M, Haimel M, Coghlan G, Corris PA, Howard LS, Kiely DG, Peacock AJ, Pepke-Zaba J, Toshner MR, Wort SJ, Gibbs JSR, Lawrie A, Gräf S, Morrell NW, Wilkins MR. Plasma metabolomics implicates modified transfer RNAs and altered bioenergetics in the outcomes of pulmonary arterial hypertension. *Circulation.* 2017;135:460–75. <https://doi.org/10.1161/CIRCULATIONAHA.116.024602>
 9. Brittain EL, Talati M, Fessel JP, Zhu H, Penner N, Calcutt MW, West JD, Funke M, Lewis GD, Gerszten RE, Hamid R, Pugh ME, Austin ED, Newman JH, Hemnes AR. Fatty acid metabolic defects and right ventricular lipotoxicity in human pulmonary arterial hypertension. *Circulation.* 2016;133:1936–44. <https://doi.org/10.1161/CIRCULATIONAHA.115.019351>
 10. Lewis GD, Ngo D, Hemnes AR, Farrell L, Domos C, Pappagianopoulos PP, Dhakal BP, Souza A, Shi X, Pugh ME, Beloiartsev A, Sinha S, Clish CB, Gerszten RE. Metabolic profiling of right ventricular-pulmonary vascular function reveals circulating biomarkers of pulmonary hypertension. *J Am Coll Cardiol.* 2016;67:174–89. <https://doi.org/10.1016/j.jacc.2015.10.072>
 11. Chouvarine P, Giera M, Kastenmüller G, Artati A, Adamski J, Bertram H, Hansmann G. Trans-right ventricle and transpulmonary metabolite gradients in human pulmonary arterial hypertension. *Heart.* 2020;106:1332–41. <https://doi.org/10.1136/heartjnl-2019-315900>
 12. Hong J, Arneson D, Umar S, Ruffenach G, Cunningham CM, Ahn IS, Diamante G, Bhetraratana M, Park JF, Said E, Huynh C, Le T, Medzikovic L, Humbert M, Soubrier F, Montani D, Girerd B, Tréguët DA, Channick R, Saggat R, Eghbali M, Yang X. Single-cell study of two rat models of pulmonary arterial hypertension reveals connections to human pathobiology and drug repositioning. *Am J Respir Crit Care Med.* 2021;203:1006–22. 2020/10/07. <https://doi.org/10.1164/rccm.202006-21690C>
 13. Voelkel NF, Bogaard HJ. Sugen, hypoxia and the lung circulation. *Pulm Circ.* 2021;11:1–3. <https://doi.org/10.1177/20458940211051188>
 14. Dean A, Gregorc T, Docherty CK, Harvey KY, Nilsen M, Morrell NW, MacLean MR. Role of the aryl hydrocarbon receptor in Sugen 5416-induced experimental pulmonary hypertension. *Am J Respir Cell Mol Biol.* 2018;58:320–30. <https://doi.org/10.1165/rcmb.2017-02600C>
 15. Abe K, Toba M, Alzoubi A, Ito M, Fagan KA, Cool CD, Voelkel NF, McMurtry IF, Oka M. Formation of plexiform lesions in experimental severe pulmonary arterial hypertension. *Circulation.* 2010;121:2747–54. 2010/06/16. <https://doi.org/10.1161/CIRCULATIONAHA.109.927681>
 16. Rafikova O, Meadows ML, Kinchen JM, Mohny RP, Maltepe E, Desai AA, Yuan JXJ, Garcia JGN, Fineman JR, Rafikov R, Black SM. Metabolic changes precede the development of pulmonary hypertension in the monocrotaline exposed rat lung. *PLoS One.* 2016;11:e0150480. <https://doi.org/10.1371/journal.pone.0150480>
 17. Philip N, Pi H, Gadkari M, Yun X, Huetsch J, Zhang C, Harlan R, Roux A, Graham D, Shimoda L, Le A, Visovatti S, Leary PJ, Gharib SA, Simpson C, Santhanam L, Steppan J, Suresh K. Transpulmonary amino acid metabolism in the sugen hypoxia model of pulmonary hypertension. *Pulm Circ.* 2023;13:e12205. <https://doi.org/10.1002/pul2.12205>
 18. Graham BB, Kumar R, Mickael C, Kassa B, Koyanagi D, Sanders L, Zhang L, Perez M, Hernandez-Saavedra D, Valencia C, Dixon K, Harral J, Loomis Z, Irwin D, Nemkov T, D'Alessandro A, Stenmark KR, Tudor RM. Vascular adaptation of the right ventricle in experimental pulmonary hypertension. *Am J Respir Cell Mol Biol.* 2018;59:479–89. <https://doi.org/10.1165/rcmb.2018-00950C>
 19. Izquierdo-Garcia JL, Arias T, Rojas Y, Garcia-Ruiz V, Santos A, Martin-Puig S, Ruiz-Cabello J. Metabolic reprogramming in the heart and lung in a murine model of pulmonary arterial hypertension. *Front Cardiovasc Med.* 2018;5:110. <https://doi.org/10.3389/fcvm.2018.00110>
 20. Pacher P, Nagayama T, Mukhopadhyay P, Bátkai S, Kass DA. Measurement of cardiac function using pressure-volume conductance catheter technique in mice and rats. *Nat Protoc.* 2008;3:1422–34. <https://doi.org/10.1038/nprot.2008.138>
 21. Ma Z, Mao L, Rajagopal S. Hemodynamic characterization of rodent models of pulmonary arterial hypertension. *J Vis Exp.* 2016;110:e53335. <https://doi.org/10.3791/53335>
 22. Do KT, Wahl S, Raffler J, Molnos S, Laimighofer M, Adamski J, Suhre K, Strauch K, Peters A, Gieger C, Langenberg C, Stewart ID, Theis FJ, Grallert H, Kastenmüller G, Krumsiek J. Characterization of missing values in untargeted MS-based metabolomics data and evaluation of missing data handling strategies. *Metabolomics.* 2018;14:128. <https://doi.org/10.1007/s11306-018-1420-2>
 23. Armitage EG, Godzien J, Alonso-Herranz V, López-González Á, Barbas C. Missing value imputation strategies for metabolomics data. *Electrophoresis.* 2015;36:3050–60. <https://doi.org/10.1002/elps.201500352>
 24. Mendez KM, Reinke SN, Broadhurst DI. A comparative evaluation of the generalised predictive ability of eight machine learning algorithms across ten clinical metabolomics data sets for binary classification. *Metabolomics.* 2019;15:150. <https://doi.org/10.1007/s11306-019-1612-4>
 25. Reinke SN, Chaleckis R, Wheelock CE. Metabolomics in pulmonary medicine: extracting the most from your data. *Eur Respir J.* 2022;60:2200102. <https://doi.org/10.1183/13993003.00102-2022>

26. Bijlsma S, Bobeldijk I, Verheij ER, Ramaker R, Kochhar S, Macdonald IA, van Ommen B, Smilde AK. Large-scale human metabolomics studies: a strategy for data (pre-) processing and validation. *Anal Chem*. 2006;78:567–74. <https://doi.org/10.1021/ac051495j>
27. Liu J, Liang G, Siegmund KD, Lewinger JP. Data integration by multi-tuning parameter elastic net regression. *BMC Bioinform*. 2018;19:369. <https://doi.org/10.1186/s12859-018-2401-1>
28. Cho S, Kim K, Kim YJ, Lee JK, Cho YS, Lee JY, Han BG, Kim H, Ott J, Park T. Joint identification of multiple genetic variants via elastic-net variable selection in a genome-wide association analysis. *Ann Hum Genet*. 2010;74:416–28. <https://doi.org/10.1111/j.1469-1809.2010.00597.x>
29. Xia J, Wishart DS. MSEA: a web-based tool to identify biologically meaningful patterns in quantitative metabolomic data. *Nucleic Acids Res*. 2010;38:W71–7. 2010/05/12. <https://doi.org/10.1093/nar/gkq329>
30. Barrett T, Wilhite SE, Ledoux P, Evangelista C, Kim IF, Tomashevsky M, Marshall KA, Phillippy KH, Sherman PM, Holko M, Yefanov A, Lee H, Zhang N, Robertson CL, Serova N, Davis S, Soboleva A. NCBI GEO: archive for functional genomics data sets—update. *Nucleic Acids Res*. 2012;41:D991–5. <https://doi.org/10.1093/nar/gks1193>
31. Chong J, Yamamoto M, Xia J. MetaboAnalystR 2.0: from raw spectra to biological insights. *Metabolites*. 2019;9:57. <https://doi.org/10.3390/metabo9030057>
32. Chong J, Xia J. MetaboAnalystR: an R package for flexible and reproducible analysis of metabolomics data. *Bioinformatics*. 2018;34:4313–4. <https://doi.org/10.1093/bioinformatics/bty528>
33. Zhao YD, Chu L, Lin K, Granton E, Yin L, Peng J, Hsin M, Wu L, Yu A, Waddell T, Keshavjee S, Granton J, de Perrot M. A biochemical approach to understand the pathogenesis of advanced pulmonary arterial hypertension: metabolomic profiles of arginine, Sphingosine-1-Phosphate, and heme of human lung. *PLoS One*. 2015;10:e0134958. <https://doi.org/10.1371/journal.pone.0134958>
34. Mura M, Cecchini MJ, Joseph M, Granton JT. Osteopontin lung gene expression is a marker of disease severity in pulmonary arterial hypertension. *Respirology*. 2019;24:1104–10. <https://doi.org/10.1111/resp.13557>
35. Ralphe J. Localization and function of the brain excitatory amino acid transporter type 1 in cardiac mitochondria. *J Mol Cell Cardiol*. 2004;37:33–41. <https://doi.org/10.1016/j.yjmcc.2004.04.008>
36. Dumas SJ, Bru-Mercier G, Courboulin A, Quatredeniens M, Rücker-Martin C, Antigny F, Nakhleh MK, Ranchoux B, Gouadon E, Vinhas MC, Vocelle M, Raymond N, Dorfmueller P, Fadel E, Perros F, Humbert M, Cohen-Kaminsky S. NMDA-type glutamate receptor activation promotes vascular remodeling and pulmonary arterial hypertension. *Circulation*. 2018;137:2371–89. <https://doi.org/10.1161/CIRCULATIONAHA.117.029930>
37. Dong YN, Hsu FC, Koziol-White CJ, Stepanova V, Jude J, Gritsiuta A, Rue R, Mott R, Coulter DA, Panettieri RA, Krymskaya VP, Takano H, Goncharova EA, Goncharov DA, Cines DB, Lynch DR. Functional NMDA receptors are expressed by human pulmonary artery smooth muscle cells. *Sci Rep*. 2021;11:8205. <https://doi.org/10.1038/s41598-021-87667-0>
38. Xiao G, Wang T, Zhuang W, Ye C, Luo L, Wang H, Lian G, Xie L. RNA sequencing analysis of monocrotaline-induced PAH reveals dysregulated chemokine and neuroactive ligand receptor pathways. *Aging*. 2020;12:4953–69. <https://doi.org/10.18632/aging.102922>
39. Lingeshwar P, Kaur G, Singh N, Singh S, Mishra A, Shukla S, Ramakrishna R, Laxman TS, Bhatta RS, Siddiqui HH, Hanif K. A study on the involvement of GABA-transaminase in MCT induced pulmonary hypertension. *Pulm Pharmacol Ther*. 2016;36:10–21. <https://doi.org/10.1016/j.pupt.2015.11.002>
40. Yu Q, Tai YY, Tang Y, Zhao J, Negi V, Culley MK, Pilli J, Sun W, Brugger K, Mayr J, Saggari R, Saggari R, Wallace WD, Ross DJ, Waxman AB, Wendell SG, Mullett SJ, Sembrat J, Rojas M, Khan OF, Dahlman JE, Sugahara M, Kagiya N, Satoh T, Zhang M, Feng N, Gorcsan J, Vargas SO, Haley KJ, Kumar R, Graham BB, Langer R, Anderson DG, Wang B, Shiva S, Bertero T, Chan SY. BOLA (Bola Family Member 3) deficiency controls endothelial metabolism and glycine homeostasis in pulmonary hypertension. *Circulation*. 2019;139:2238–55. <https://doi.org/10.1161/CIRCULATIONAHA.118.035889>
41. Schwörer S, Pavlova NN, Cimino FV, King B, Cai X, Sizemore GM, Thompson CB. Fibroblast pyruvate carboxylase is required for collagen production in the tumour microenvironment. *Na Metab*. 2021;3:1484–99. <https://doi.org/10.1038/s42255-021-00480-x>
42. Certo M, Tsai CH, Pucino V, Ho PC, Mauro C. Lactate modulation of immune responses in inflammatory versus tumour microenvironments. *Nat Rev Immunol*. 2021;21:151–61. <https://doi.org/10.1038/s41577-020-0406-2>

SUPPORTING INFORMATION

Additional supporting information can be found online in the Supporting Information section at the end of this article.

How to cite this article: Simpson CE, Ambade AS, Harlan R, Roux A, Graham D, Klauer N, Tuhy T, Kolb TM, Suresh K, Hassoun PM, Damico RL. Spatial and temporal resolution of metabolic dysregulation in the Sugen hypoxia model of pulmonary hypertension. *Pulm Circ*. 2023;13:e12260. <https://doi.org/10.1002/pul2.12260>